CHAPTER-5

Can Carbene Decorated [FeFe]-Hydrogenase Model Complexes Catalytically Produce Dihydrogen? An Insight from Theory.

Abstract: In this chapter, we have studied the mechanistic details of catalytic production of dihydrogen using bio-inspired [FeFe]–hydrogenase model complexes which possess rotated conformation at one of the iron centers. The catalytic evolution of H_2 is found to be highly favourable using both the complexes as evident from high exergonicity of the overall reaction as well as very shallow activation energy barrier for the transition states involved. The computed reduction potential values are found to be less negative compared to those reported earlier for experimentally known system.

[5.1] Introduction

Dihydrogen production has been an active area of research for a long time due to its possible use as energy resource. In nature, the enzyme known as hydrogenase is known to effectively catalyze the reversible production of dihydrogen. Accordingly, extensive research work has been performed toward designing of model complexes which can replicate the catalytic activity of this enzyme [1]. The native enzyme is classified into three main categories *viz.* [FeFe]-, [NiFe]- and [Fe]- hydrogenase on the basis of the metal ion composition in their active sites [2,3]. Between the bimetallic ones, [FeFe]-hydrogenase is reported to be more effective in proton reduction compared to [NiFe]-hydrogenase [4]. The active site of [FeFe]-hydrogenase (Scheme 5.1) contains a bimetallic subcluster $[2Fe]_H$ which is linked to a ferredoxin-like Fe_4S_4 cubane through a cystenyl sulphur atom [5]. Both the iron centers in $[2Fe]_H$ (known as proximal (Fe_p) and

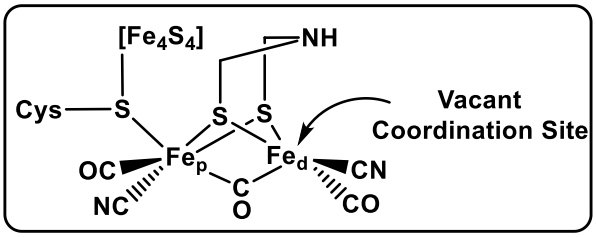

Scheme 5.1: Schematic representation of the active site of [FeFe]-hydrogenase.

distal (Fe_d) with respect to the Fe_4S_4 cubane) are bound to abiological ligands CO and CN^- as well as an azadithiolate bridge which connects both the iron centers [6]. The two resting states of the active site of [FeFe]-hydrogenase are termed as H_{ox} and H_{red} and both these states feature a bridging CO group between Fe_p and Fe_d [3b-e,5,7]. The H_{ox} state ($Fe^{II}Fe^{I}$) is known to operate in the direction of H_2 splitting while H_{red} state ($Fe^{I}Fe^{I}$) is ready to accept protons and proceed toward reductive direction. In both these states, the vacant coordination site at Fe_d which is in trans position with respect to the μ-CO group is the possible coordination site for incoming H_2/H^+ [8].

Till date a number of studies have been carried out towards understanding the mechanistic details of proton reduction as well as dihydrogen splitting using biomimetic model complexes [9]. The primary modifications in these model complexes are the use of phosphine based ligands as well as the use of an electrode in place of the redox-active Fe_4S_4 cubane cluster. The major problems encountered in these models are the high values of over potentials as well as the instability of the rotated conformation at one of

the iron center which is an important structural requirement for efficient catalytic production of dihydrogen. However, till date only a few model complexes were isolated in the reduced $Fe^{I}Fe^{I}$ state which possess vacant coordination site at one of the iron center and low temperature NMR experiments suggested that one of them (**[2]^{0}**, Scheme 5.2) results in the formation of a terminal hydride upon protonation thereby indicating the basic nature of the rotated iron center [10]. Interestingly, as described in the previous chapter, we were able to computationally characterize model complexes having a rotated geometry at one of the iron center by suitably modifying the coordination sphere with a combination of azadithiolate bridge and chelated CAAC. Further, even though a number of studies were carried out toward understanding the mechanistic details of electrocatalytic proton reduction using different biomimetic model complexes, there were no such reports using a model complex which features a rotated conformation in the reduced state. Herein, we report for the first time, the complete mechanism of catalytic production of dihydrogen using a carbene stabilized model complex with a rotated geometry (**[1]^{0}**, Scheme 5.2) and its comparison with the experimentally known model complex (**[2]^{0}**).

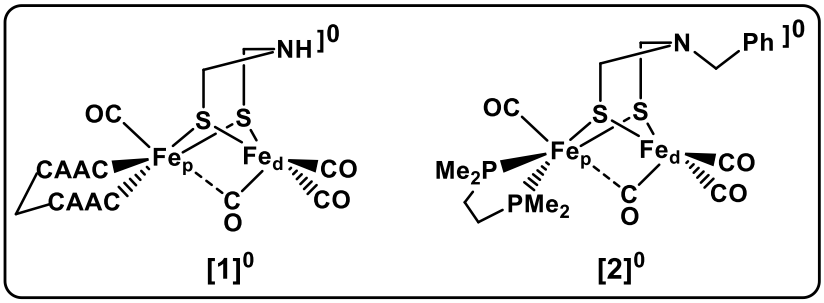

Scheme 5.2: Schematic representation of the model complexes used as catalyst in the present study for production of dihydrogen.

[5.2] Computational Details

Density functional theory calculations were performed to optimize all the molecules in solvent phase (CH_2Cl_2) using the M062X functional in conjunction with the Def2-TZVP basis set for all the atoms [11,12]. This level of theory is used for all the other calculations unless otherwise stated. In order to mimic the experimental conditions, solvent effects were incorporated using the polarizable continuum model (PCM) [13]. Further, dispersion effects were evaluated using D3 version of Grimme's dispersion correction coupled with D3 damping function using the keyword "Empirical Dispersion

= GD3". Frequency calculations were carried out to characterize the nature of the stationary points on the potential energy surface. All the ground state structures were characterized with real vibrational frequencies while the transition states were found to have only one imaginary frequency. The transition states were further verified by intrinsic reaction coordinate (IRC) analysis. Free energies corresponding to the reduction and protonation steps were calculated relative to the processes $[Cp^*_2Cr] \rightarrow [Cp^*_2Cr]^+ + e^-$ and $HBF_4.Et_2O \rightarrow BF_4^-.Et_2O + H^+$ respectively, without any structural simplification of the molecules involved ($[Cp^*_2Cr]$ is decamethyl chromocene). The nature of bonding was ascertained by performing Natural Bond Orbital (NBO) [14] analysis as implemented in the Gaussian 09 suit of program [15].

In order to get an idea about the electronic changes at the iron centres throughout the catalytic cycle, we calculated the ^{57}Fe Mössbauer parameters using the ORCA 4.0 program [16]. For this, initially all the complexes were fully optimized at B3LYP/TZVP level of theory [17,18]. These optimized structures were used to calculate the isomer shift (δ) value by employing the TZVP basis set for all the main group elements while the enlarged CP(PPP) basis set [19] for the iron atoms. We have used the linear equation $\delta = \alpha(\rho - C) + \beta$ to calculate the isomer shift values, where ρ is the total electron density on iron nuclei and α, β and C are constants whose values were adopted from previous studies [20].

We have calculated the pK_a values using the relationship, pK_a = $\Delta G°(H^+)/(RT\ln 10)$ where the term $\Delta G°(H^+)$ is the reaction free energy for deprotonation, R is the gas constant and T = 298 K [9i]. However, due to the unavailability of similar experimental reference systems as well as to avoid the determination of the free energy of the solvated proton, we calculated the difference in pK_a values (i.e., ΔpK_a) for the protonated states.

Further, the BP86 functional [21] was adopted to calculate the absolute redox potential (E_{abs}), using the Nernst equation $\Delta G = -nFE_{abs}$, where n is the number of electrons involved and F is the Faraday constant. The calculated absolute reduction potential values were referenced to the standard reduction potential for the ferrocene/ferrocinium couple calculated at the same level of theory. The choice of BP86 functional instead of M062X is based on the good quality of redox potentials computed at BP86 level of theory in previous reports [22]. Further, the computed absolute

reduction potential for the ferrocene/ferrocinium couple at BP86 level (5.1) is found to be closest to that previously reported in literature (5.05) [22].

[5.3] Results and Discussion

Before discussing the results, it is necessary to give a description about the nomenclature of the model complexes investigated in this study. The parent carbene substituted neutral complex is denoted by **[1]^0** while the experimentally known one with dmpe (1,2-bis(dimethylphosphino)ethane) ligand is named as **[2]^0** (Scheme 5.2). In this notation, the overall charge of the complex is written outside the square bracket as superscript. Further, the azadithiolate protonated species is abbreviated as **[1-*adt*H]$^+$** while the terminal hydride as **[1-*t*H]$^+$**. A similar nomenclature is followed for complexes of **[2]^0**.

[5.3.1] Hydrogen Evolution Catalyzed by [1]^0

The structural flexibility of the active site of the native [FeFe]-hydrogenase plays a crucial role during reversible reduction of protons to molecular hydrogen. Interestingly, the starting complex **[1]^0** adopts an inverted square pyramidal geometry at one of the iron centers (Scheme 5.2) and results in the evolution of molecular hydrogen upon alternate addition of two equivalents of protons and electrons as shown in Scheme 5.3. Even though the first protonation may directly lead to the terminal hydride **[1-*t*H]$^+$**, one cannot rule out the possibility of azadithiolate protonation (i.e., protonation at the bridgehead nitrogen atom) as the reaction is found to be exergonic (*vide infra*). Initial protonation leads to an increase in Fe_p-Fe_d bond length by 0.02 Å (Table 5.1) as well as decrease in the extent of bridging of the carbonyl group as evident from an increase in Fe_p-CO_{bridg} bond length which is further corroborated from an increase in carbonyl stretching frequency (by 58 cm^{-1}) for this semi- bridging CO group. The second step involves intramolecular proton transfer from the azadithiolate bridgehead nitrogen atom to the vacant apical site of the distal iron center thereby forming a terminal hydride **[1-*t*H]$^+$** which is followed by reduction with first equivalent of Cp^*_2Cr. A molecular orbital (MO) analysis shows that the lowest unoccupied molecular orbital (LUMO) in **[1-*t*H]$^+$** has antibonding contribution from both the iron centers (Figure 5.1) and accordingly, upon reduction, the Fe_p-Fe_d bond length gets significantly elongated in **[1-*t*H]^0** compared to that in **[1-*t*H]$^+$** (Table 5.1). Further, in **[1-*t*H]^0** the carbonyl group between the iron centers came to a completely bridging position as evident from similar Fe_p-CO_{bridg} and

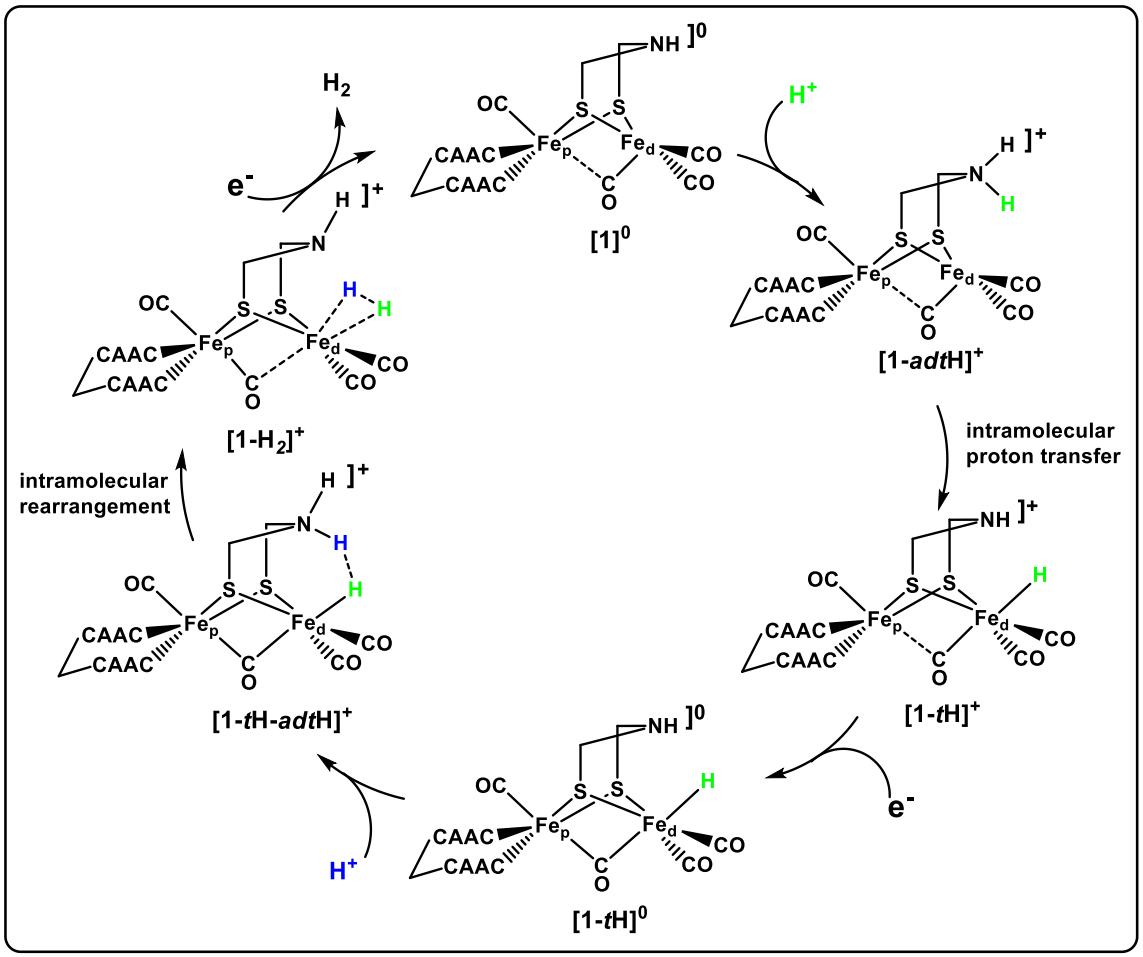

Scheme 5.3: Schematic representation of the catalytic cycle of H_2 production catalyzed by **[1]^0**.

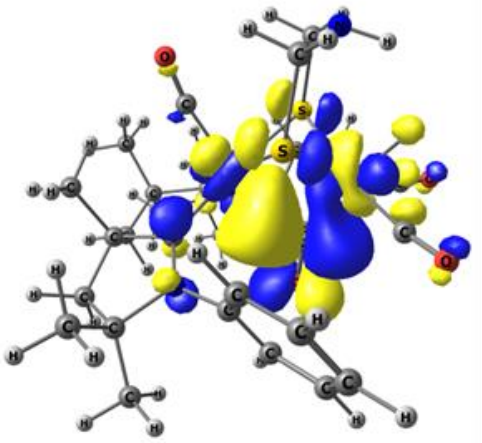

Figure 5.1: Lowest Unoccupied Molecular Orbital (LUMO) of **[1-*t*H]$^+$**.

Table 5.1: M062X/Def2-TZVP calculated values of key geometrical parameters for both the complexes **[1]^0** and **[2]^0** and the intermediates involved in the catalytic cycle. The iron centers are denoted by Fe_p and Fe_d whereas the apical and bridging carbonyl groups are indicated by CO_{ap} and CO_{bridg} respectively.

Complex	Fe_p-Fe_d	Fe_p-CO_{ap}	Fe_p-CO_{bridg}	Fe_d-CO_{bridg}	Fe_d-H	H-H
[1]^0	2.617	1.874	2.305	1.771	-	-
[1-*adt*H]$^+$	2.638	1.887	2.384	1.772	-	-
[1-*t*H]$^+$	2.755	1.887	2.455	1.952	1.515	-
[1-*t*H]^0	2.860	1.936	2.051	2.115	1.589	-
[1-*t*H-*adt*H]$^+$	2.880	1.951	2.063	2.123	1.611	1.552
[1-H_2]$^+$	3.117	1.918	1.939	2.900	2.214 2.182	0.755
[2]^0	2.605	1.858	2.188	1.779	-	-
[2-*adt*H(a)]$^+$	2.608	1.866	2.264	1.767	-	-
[2-*adt*H(b)]$^+$	2.612	1.865	2.645	1.758	-	-
[2-*t*H]$^+$	2.743	1.900	1.925	2.443	1.491	-
[2-*t*H]^0	2.811	1.917	2.051	2.078	1.561	-
[2-*t*H-*adt*H(a)]$^+$	2.840	1.932	2.027	2.091	1.563	-
[2-*t*H-*adt*H(b)]$^+$	2.843	1.932	2.078	2.083	1.607	1.565
[2-H_2]$^+$	3.113	1.910	1.928	2.809	2.154 2.124	0.756

Fe_d-CO_{bridg} bond lengths. The next step is the protonation of **[1-*t*H]^0** at the bridgehead nitrogen atom thereby generating an ammonium hydride (**[1-*t*H-*adt*H]$^+$**) which is accompanied by a slight increase in Fe_p-Fe_d bond length (~0.02Å). It should be noted that the shift in ν_{CO} value for the bridging CO group (23 cm^{-1}) as a result of *N*-protonation (i.e., **[1-*t*H]^0** vs **[1-*t*H-*adt*H]$^+$**) is comparable to that observed experimentally (20 cm^{-1}) in similar systems [23]. Further, in this diprotonated species, the computed dihydrogen distance (1.552 Å) is comparable to the previously reported value (1.55 Å) [9i] and lies within twice the van der Walls radius of hydrogen thereby indicating dihydrogen bonding. In the next step, **[1-*t*H-*adt*H]$^+$** undergoes rearrangement resulting in the formation of a non-classically bonded dihydrogen complex (**[1-H_2]$^+$**). The major structural change during this rearrangement is the significant elongation of the Fe_p-Fe_d bond as well as shifting of the bridging CO to a semi-bridging position where it strongly binds to Fe_p rather than Fe_d. The catalytic cycle is completed with the liberation of H_2

and regeneration of the catalyst **[1]^0** upon addition of the second equivalent of reductant (Cp^*_2Cr).

[5.3.2] Hydrogen Evolution Catalyzed by [2]^0

We have also considered the experimentally known complex **[2]^0** and studied the complete catalytic cycle of H_2 evolution using this complex. The steps involved in case of **[2]^0** (Scheme 5.4) are quite similar to those observed with **[1]^0**. The first step is the *N*-protonation at the azadithiolate bridgehead which results in the formation of the ammonium complex (**[2-*adt*H(a)]$^+$**). However, unlike in **[1-*adt*H]$^+$**, the proton occupies an equatorial position in **[2-*adt*H(a)]$^+$**. Therefore, this catalytic cycle involves an additional step where **[2-*adt*H(a)]$^+$** undergoes rearrangement to an intermediate (**[2-*adt*H(b)]$^+$**) in which the proton is suitably placed for transfer to Fe_d atom favouring the

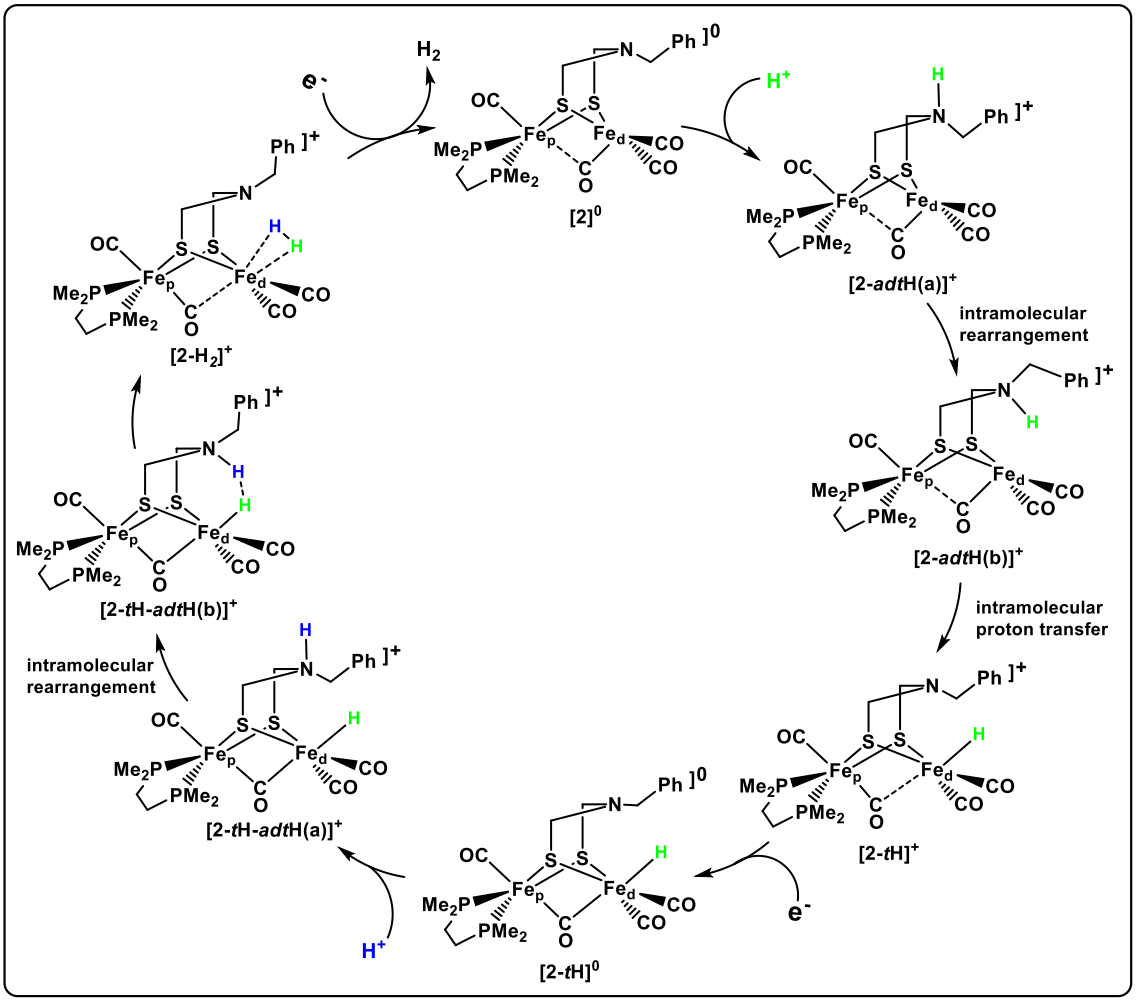

Scheme 5.4: Schematic representation of the catalytic cycle of H_2 production catalyzed by **[2]^0**.

formation of terminal hydride (**[2-*t*H]**$^+$). In **[2-*t*H]**$^+$, the Fe_p-Fe_d bond length is significantly longer than that in **[2-*adt*H(a)]**$^+$ and **[2-*adt*H(b)]**$^+$. However, unlike in **[1-*t*H]**$^+$, in **[2-*t*H]**$^+$ the semi-bridging CO is strongly bonded to Fe_p rather than Fe_d. This may be attributed to the stronger interaction between Fe_d and the apical hydrogen atom in **[2-*t*H]**$^+$ compared to that in **[1-*t*H]**$^+$ (Table 5.1). Further, the stronger interaction between the semi-bridging carbonyl and Fe_p in **[2-*t*H]**$^+$ is also supported by the increase in Fe_p-CO_{ap} bond length. Addition of the first equivalent of the reductant (Cp^*_2Cr) leads to the formation of **[2-*t*H]^0** which yields the ammonium hydride (**[2-*t*H-*adt*H(a)]**$^+$) upon treatment with proton source ($HBF_4.Et_2O$). This is followed by rearrangement of the azadithiolate bridge thereby bringing the equatorial hydrogen atom to a position in which it can effectively interact with the terminal hydride (**[2-*t*H-*adt*H(b)]**$^+$). The H···H bond distance in **[2-*t*H-*adt*H(b)]**$^+$ (1.565Å) is comparable to that computed for **[1-*t*H-*adt*H]**$^+$ (1.552Å). Both protonation of **[2-*t*H]^0** as well as rearrangement of **[2-*t*H-*adt*H(a)]**$^+$ to **[2-*t*H-*adt*H(b)]**$^+$ are found to shift the ν_{CO} value for the bridging CO by almost 18 cm^{-1} to higher energy. Similar to the case with **[1]^0**, here also we could get an intermediate where the dihydrogen molecule is non-classically bonded to the distal iron center (**[2-H_2]**$^+$) which upon reduction results in the formation of free H_2 as well as regeneration of the catalyst **[2]^0**.

[5.3.3] Mechanistic Details for H_2 Evolution Using [1]^0 and [2]^0

In addition to the intermediates involved in the catalytic liberation of H_2 using **[1]^0** (as discussed in the previous sections), we also characterized all the possible transition states and the mechanistic steps are depicted in Figure 5.2. Our calculations suggest that the catalytic production of H_2 using **[1]^0** is a highly exergonic ($\Delta G = -73.4$ kcal mol^{-1}) process. The first *N*-protonation step leading to the ammonium complex **[1-*adt*H]**$^+$ is found to be favourable by 8.0 kcal mol^{-1} which isomerizes to the terminal hydride **[1-*t*H]**$^+$ *via* a transition state (**TS1$_{[1]}^0$**) with activation energy barrier of 4.8 kcal mol^{-1}. Interestingly, this intramolecular proton transfer step is also facile as indicated by the calculated negative change in Gibbs free energy by 8.8 kcal mol^{-1}. The next step which is the reduction with first equivalent of Cp^*_2Cr is found to be considerably exergonic with $\Delta G = -16.3$ kcal mol^{-1}. Interestingly, the computed Mulliken spin density values for **[1-*t*H]^0** indicate that ~ 50% of the total spin is equally distributed on both the iron centers (0.263 and 0.260 on Fe_p and Fe_d respectively) while the remaining 50% is on

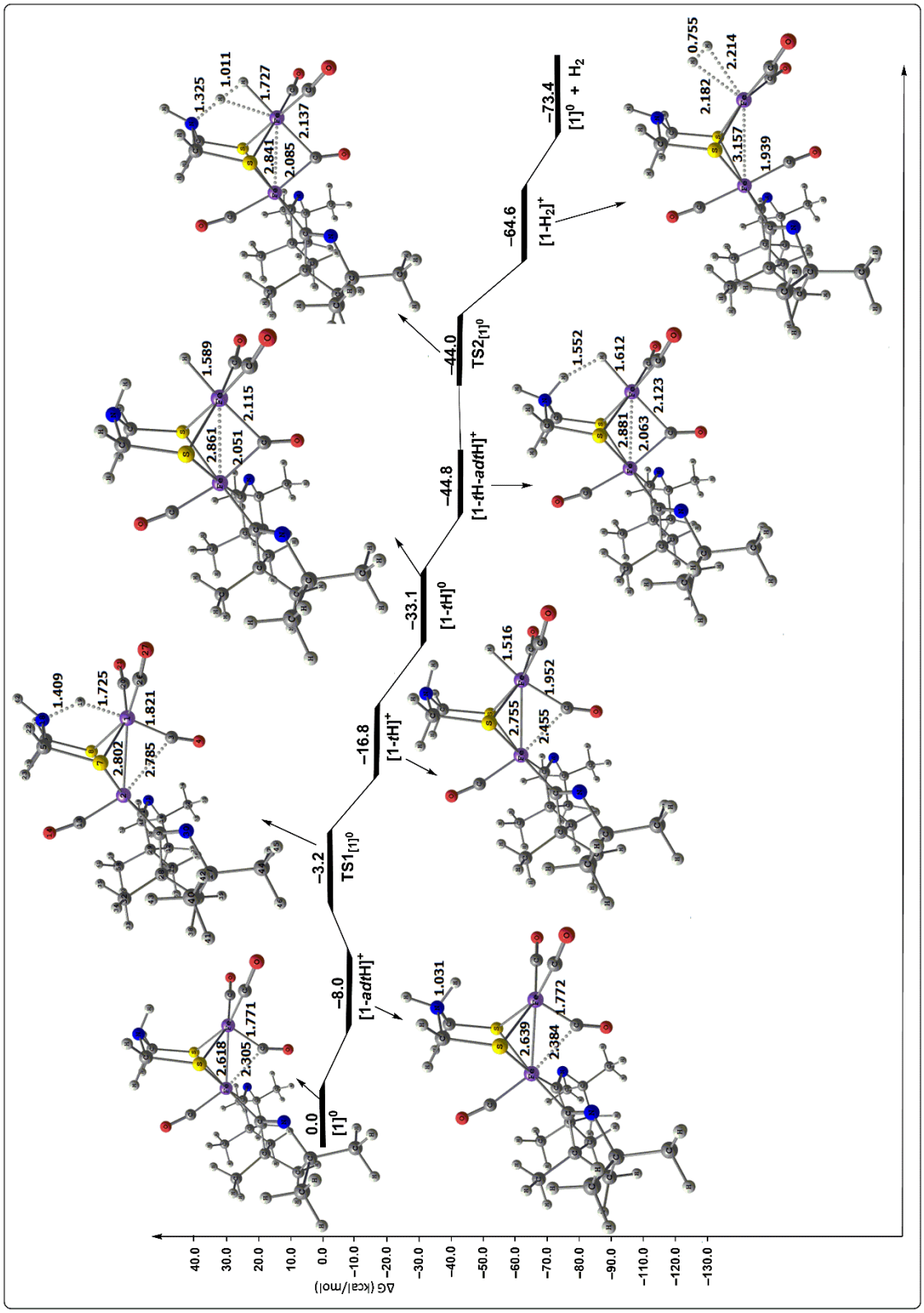

Figure 5.2: Proposed mechanism for production of H_2 using **[1]^0** (phenyl groups at the nitrogen atoms of CAAC are omitted for clarity.)

the bridging carbonyl group (0.503). This equal distribution of spin densities on both the iron centers lead to more symmetric coordination of the bridging CO group in the reduced species. A closer look at Figure 5.2 indicate that reduction not only increases the Fe_p-Fe_d bond length in **[1-*t*H]^0** but also significantly increases the Fe_d-H bond length. This can be attributed to the fact that the LUMO of **[1-*t*H]$^+$** (Figure 5.1) not only has antibonding interaction between the two iron centers but also has some contribution from the Fe_d-H bond which is antibonding in nature. The second protonation which leads to the formation of the ammonium hydride **[1-*t*H-*adt*H]$^+$** is accompanied by an energy release of 11.7 kcal mol^{-1}. This doubly protonated species also maintains the symmetric coordination mode of the bridging CO group which is consistent with nearly equal spin densities on both Fe_p and Fe_d (0.251 and 0.286 respectively) centers. **[1-*t*H-*adt*H]$^+$** also features the incipient formation of a dihydrogen bond between the azadithiolate proton and hydride at Fe_d which then undergoes an intramolecular proton transfer to form **[1-H$_2$]$^+$** through transition state (**TS2$_{[1]}^0$**) involving a barrier of only 0.8 kcal mol^{-1}. It should be noted that the energy required to overcome the barrier involved in both the intramolecular proton transfer processes are very minimal thereby indicting the high efficiency of the catalyst **[1]^0** toward catalytic production of H_2. While previous studies suggested higher stability for the mixed valence doubly protonated species compared to the weakly bound H_2-adduct [9i], our studies indicate higher stability (by 19.8 kcal mol^{-1}) for the non-classically bound dihydrogen complex (**[1-H$_2$]$^+$**) over the isomeric ammonium hydride (**[1-*t*H-*adt*H]$^+$**). Further, the computed Mulliken spin density values shows that the total spin is entirely localized on the distal Fe center thereby suggesting the mixed valence Fe_p(II)Fe_d(I) oxidation state assignment for **[1-H$_2$]$^+$** where the H_2 molecule is weakly bonded to a Fe(I) center. Interestingly, the oxidation states of the two iron centers of **[1-H$_2$]$^+$** resemble that in the H_{ox} state of the native enzyme. Further, in **[1-H$_2$]$^+$**, the bound H_2 has a bond length of 0.755Å which is marginally longer than that for free H_2 molecule (0.740Å, calculated at the same level of theory) suggesting an weakly activated H_2 molecule. The final liberation of H_2 from the loosely bound dihydrogen complex **[1-H$_2$]$^+$** as a result of addition of second equivalent of reductant is also found to be exergonic by −8.8 kcal mol^{-1}.

For a comparison purpose, we have also studied the mechanistic details of catalytic production of H_2 using **[2]^0** and the steps are depicted in Figure 5.3. The initial *N*-protonation as well as subsequent isomerization to **[2-*adt*H(b)]$^+$** are found to be

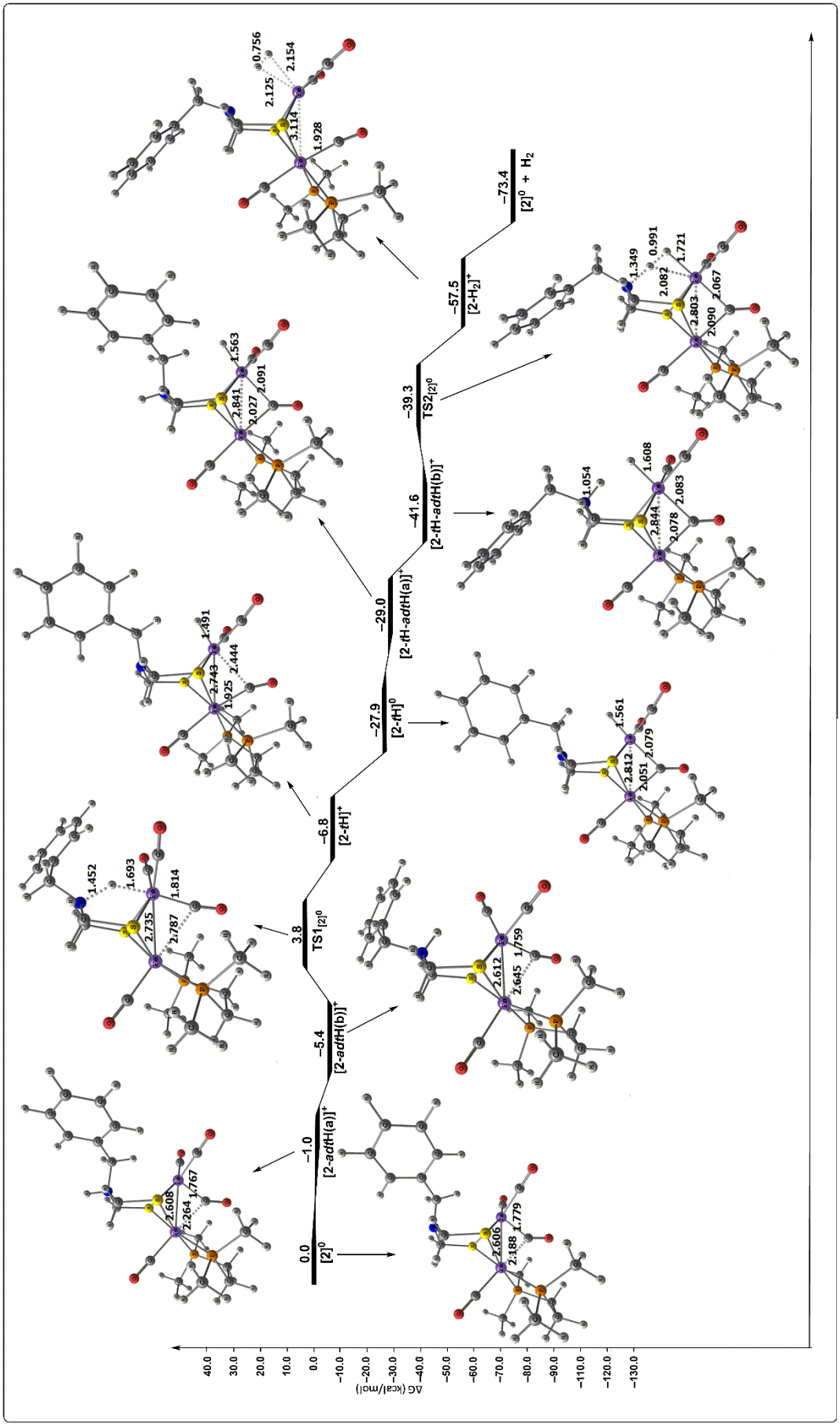

Figure 5.3: Proposed mechanism for production of H_2 using **[2]^0**

exergonic in nature (by −1.0 and −4.4 kcal mol^{-1} respectively). It should be noted that while the Fe_d center adopts a complete inverted square pyramidal geometry in both **[2]^0** and **[2-*adt*H(b)]$^+$**, the same is distorted to some extent in **[2-*adt*H(a)]$^+$**. This may be attributed to the absence of agostic interaction between the bulky azadithiolate substituent and the distal iron center which is responsible for the stabilization of the rotated structure in Fe(I)Fe(I) state. The terminal hydride formation is found to be favourable by 1.4 kcal mol^{-1} which involves a transition state (**TS1$_{[2]}^0$**) with an activation energy barrier of 9.2 kcal mol^{-1}. A comparison with Figure 5.2 shows that the energy barrier for this intramolecular proton transfer is higher in **[2]^0** compared to that in **[1]^0**. However, reduction of the terminal hydride (**[2-*t*H]$^+$**) is computed to be more exergonic (ΔG = −21.1 kcal mol^{-1}) as compared to that in **[1]^0** (ΔG = −16.3 kcal mol^{-1}) which may be attributed to the electron rich nature of the diiron core in **[1]^0** rendered by the presence of better electron donating chelated CAAC ligands. Further, as evident from the calculated Mulliken spin densities, the distribution of the total spin in **[2-*t*H]^0** (~ 50% on both the iron centers and ~ 50% on the bridging CO) is akin to that in **[1-*t*H]^0**. Similar to the first protonation, the formation of the doubly protonated species (**[2-*t*H-*adt*H(a)]$^+$**) is also marginally exergonic (ΔG = −1.1 kcal mol^{-1}). However, the isomerisation of **[2-*t*H-*adt*H(a)]$^+$** to **[2-*t*H-*adt*H(b)]$^+$** is significantly exergonic in nature (ΔG = −12.6 kcal mol^{-1}). This is followed by an intramolecular proton transfer process involving **TS2$_{[2]}^0$** which leads to the weakly bound dihydrogen complex **[2-H$_2$]$^+$**. Interestingly, similar to the case with **[1]^0**, here also the formation of this non-classical dihydrogen complex **[2-H$_2$]$^+$** is almost a barrier less process ($\Delta G^{\#}$ = +2.3 kcal mol^{-1}). Further, the H···H bond length in **[2-H$_2$]$^+$** is 0.756Å which is equal to that obtained in **[1-H$_2$]$^+$**. Similar to **[1-H$_2$]$^+$**, **[2-H$_2$]$^+$** also contains a mixed valence Fe(II)Fe(I) core as indicated by the calculated Mulliken spin density values (0.014 on Fe_p and 1.118 on Fe_d).

[5.3.4] Mössbauer Spectroscopy and Mulliken Spin Densities

In order to get an insight about the change in electron density around the metal centers during the catalytic production of H_2 using both **[1]^0** and **[2]^0**, we have calculated the Mössbauer isomer shift (δ) values (Table 5.2). In addition, we also evaluated the values of Mulliken spin density for the complexes with unpaired electrons (Table 5.2). Similar to the H_{red} state of the native enzyme, both the iron centers in the starting complex **[1]^0** are believed to be in a low spin Fe(I) state. However, the ^{57}Fe isomer shift

Table 5.2: Calculated values of Mössbauer isomer shift (δ) and Mulliken spin densities (ρ).

Complex	Fe_p		Fe_d		CO_{bridg}
	δ	P	δ	ρ	ρ
[1]^0	0.201	-	0.013	-	-
[1-*adt*H]$^+$	0.227	-	0.053	-	-
[1-*t*H]$^+$	0.159	-	-0.004	-	-
[1-*t*H]^0	0.241	0.263	0.049	0.260	0.503
[1-*t*H-*adt*H]$^+$	0.258	0.251	0.131	0.286	0.488
[1-H_2]$^+$	0.145	0.012	0.352	1.143	-0.001
[2]^0	0.218	-	0.020	-	-
[2-*adt*H(a)]$^+$	0.232	-	0.072	-	-
[2-*adt*H(b)]$^+$	0.202	-	0.059	-	-
[2-*t*H]$^+$	0.215	-	-0.001	-	-
[2-*t*H]^0	0.272	0.311	0.031	0.218	0.473
[2-*t*H-*adt*H(a)]$^+$	0.287	0.326	0.088	0.211	0.455
[2-*t*H-*adt*H(b)]$^+$	0.280	0.286	0.106	0.244	0.477
[2-H_2]$^+$	0.163	0.014	0.364	1.118	-0.005

(δ) value for Fe_p is found to be significantly positive compared to that for Fe_d which may be attributed to the presence of chelated CAAC ligand at Fe_p. By virtue of its strong electron donation ability, CAAC increases the d-electron density at the proximal iron centre which results in more positive δ values due to the increased shielding of the s-electrons by d-electrons. Similar is the case for all the intermediates (except **[1-H_2]$^+$**) involved in the catalytic evolution of H_2 using **[1]^0**. A comparison between **[1]^0** and **[1-*t*H]$^+$** shows that formation of the terminal hydride lowers the isomer shift values for both the iron centers. This is in accordance with decrease of d-electron density at both Fe_p and Fe_d thereby supporting the Fe_p(II)Fe_d(II) assignment for this terminal hydride species. The decrease in electron density at the iron centers is also evident from the higher average ν_{CO} value for **[1-*t*H]$^+$** (2209 cm^{-1}) compared to that for **[1]^0** (2033 cm^{-1}). Further, reduction of **[1-*t*H]$^+$** leads to more positive δ values for both Fe_p and Fe_d (i.e., in **[1-*t*H]^0**) indicating reduction of both the metal centers which is further supported by the calculated Mulliken spin density values (ρ) as almost 50% of the reducing equivalent is delocalized between both the iron centres while the rest 50% is on the bridging CO group. This is also the case with **[1-*t*H-*adt*H]$^+$** where the spin is also delocalized between

both the iron centres as well as on the bridging CO group. However, similar to the case with first prtonation (i.e., in **[1-*adt*H]**$^+$) there is a positive shift of the δ values on going from **[1-*t*H]**^{0} to **[1-*t*H-*adt*H]**$^+$ which may be because of the better σ-electron withdrawing nature of the ammonium centre. Interestingly, among all the intermediates involved in the catalytic cycle, only **[1-H$_2$]**$^+$ possesses more positive isomer shift value for Fe_d compared to that for Fe_p. This indicates higher d-electron density at Fe_d than in Fe_p which is further supported by the localization of the total spin on the distal iron centre as evident from the calculated Mulliken spin density values. Therefore both the isomer shift values and the Mulliken spin density values support an oxidation state assignment of Fe_p(II)Fe_d(I) for **[1-H$_2$]**$^+$. Similar trend of change in δ and Mulliken spin density values are obtained for the intermediates involved in the catalytic production of H_2 using **[2]**^{0} thereby indicating similar change in electronic environment around the Fe centers throughout the catalytic cycle.

[5.3.5] Redox and Acid-Base Properties

In order to investigate the redox behaviour of the singly and doubly protonated species of both **[1]**^{0} and **[2]**^{0}, we have calculated the reduction potential (Table 5.3) for both the reduction event involved in the catalytic cycle. The calculated reduction potential for the couple **[1-*t*H]**$^+$/**[1-*t*H]**^{0} is found to be significantly negative compared to that computed for the second reduction event (**[1-H$_2$]**$^+$/**[1]**^{0}). This indicates that the reduction of the weakly bound dihydrogen complex is more favourable compared to the terminal hydride species. Similar results are also obtained for the redox couples with the dmpe substituted complex (**[2]**^{0}). However, the *E*° values calculated for the reduction events involved in the catalytic cycle of **[1]**^{0} are found to be less positive compared to those for **[2]**^{0}. This can be reasoned to the presence of chelated CAAC ligands in **[1]**^{0}

Table 5.3: BP86/Def2-TZVP calculated values of reduction potentials of the reduction events for both **[1]**^{0} and **[2]**^{0}.

Redox Event	*E*° (V)
[1-*t*H]$^+$/**[1-*t*H]**^{0}	−1.41
[1-H$_2$]$^+$/**[1]**^{0}	0.10
[2-*t*H]$^+$/**[2-*t*H]**^{0}	−1.32
[2-H$_2$]$^+$/**[2]**^{0}	0.26

which renders the diiron core more electron rich compared to that in **[2]^0**. It should be noted that our calculated potential values for the reduction of the terminal hydride species in both **[1]^0** and **[2]^0** are close, indeed more favourable (i.e., less negative) than those reported for similar experimentally known system [23].

As described in the computational details section, we have calculated the ΔpK_a values for the protonated species obtained from the three different pathways shown in Scheme 5.5 and the values are listed in Table 5.4. The $\Delta pK_a(P_2\text{-}P_1)$ values for both **[1]^0**

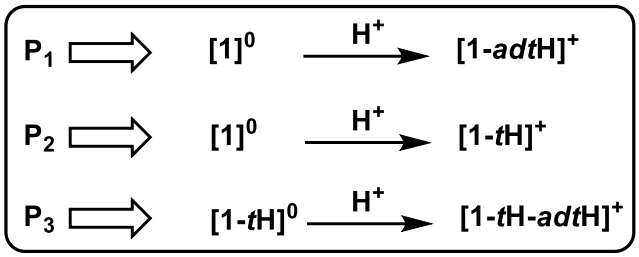

Scheme 5.5: Schematic depiction of different protonation pathways considered in this study for complex **[1]^0**. Similar pathways are also considered for **[2]^0**.

Table 5.4: M062X/Def2-TZVP calculated ΔpK_a values for the protonated species obtained from different protonation pathways.

ΔpK_a	**[1]^0**	**[2]^0**
P_2-P_1	6.5	4.2
P_3-P_2	−4.3	−4.1
P_3-P_1	2.2	0.1

and **[2]^0** are found to be positive which indicates that the distal iron center is more basic than the amine group of the azadithiolate bridge which is in tune with previous experimental and theoretical results [9i,23]. The higher basicity of Fe_d center is further supported by the calculated higher natural charge at Fe_d (−1.421 and −1.264 for **[1]^0** and **[2]^0** respectively) compared to that in the amino nitrogen atom (−0.721 and −0.565 for **[1]^0** and **[2]^0** respectively). The same is also reflected in the relatively higher exergonicity associated with the formation of terminal hydride than that with the ammonium tautomer (ΔG = −16.8 and −8.0 kcal mol^{-1} for the formation of **[1-*t*H]$^+$** and **[1-*adt*H]$^+$** respectively, Figure 5.2). The computed negative $\Delta pK_a(P_3\text{-}P_2)$ values show that the ammonium hydride is more acidic compared to the terminal hydride for both **[1]^0** and **[2]^0**. Interestingly, the positive difference in the pK_a values of the first and second *N*-

protonation steps suggest that the amino nitrogen in the reduced terminal hydride (**[1-*t*H]^0**) in more basic compared to that in the parent complex (**[1]^0**) which is also reflected in the calculated natural charge values. However, in case of **[2]^0**, the $\Delta pK_a(P_3\text{-}P_1)$ value is found to be only slightly positive thereby indicating comparable basicity of the amino nitrogen atom in the reduced terminal hydride (**[2-*t*H]^0**) as well as in the parent complex (**[2]^0**).

[5.4] Conclusions

Quantum chemical calculations were carried out to understand the mechanistic details of catalytic production of dihydrogen using bio-inspired [FeFe]-hydrogenase model complexes which possess rotated conformation at one of the iron centers. The catalytic evolution of H_2 is found to be highly favourable using both the complexes as evident from high exergonicity of the overall reaction as well as very shallow activation energy barrier for the transition states involved. Interestingly, on the basis of computed Mössbauer isomer shift and Mulliken spin density values, this study provides evidence for an intermediate where dihydrogen is non-classically bonded to an iron center (Fe_d) with the total spin entirely localized on Fe_d. Most importantly, the computed reduction potential values for the model systems are found to be less negative compared to that reported earlier for similar experimentally known system. In accordance with previous experimental observations, our calculations also demonstrate the higher basicity of the distal iron center compared to the amino nitrogen atom. However, one cannot completely rule out the possibility of the amino group of the azadithiolate bridge as the initial protonation site.

[5.5] Bibliography

[1] (a) Nehring, J. L. and Heinekey, D. M. Dinuclear Iron Isonitrile Complexes: Models for the Iron Hydrogenase Active Site. *Inorganic Chemistry*, 42(14):4288-4292, 2003. (b) Capon, J. F., Hassnaoui, S. E., Gloaguen, F., Schollhammer, P., and Talarmin, J. N-Heterocyclic Carbene Ligands as Cyanide Mimics in Diiron Models of the All-Iron Hydrogenase Active Site. *Organometallics*, 24(9):2020-2022, 2005. (c) Morvan, D., Capon, J. F., Gloaguen, F., Le Goff, A., Marchivie, M., Michaud, F., Schollhammer, P., Talarmin, J., and Yaouanc, J. J. N-Heterocyclic Carbene Ligands in Nonsymmetric Diiron Models of Hydrogenase Active Sites. *Organometallics*, 26(8):2042-2052, 2007. (d) Morvan, D., Capon, J. F., Gloaguen, F., Pétillon, F. Y., Schollhammer, P., Talarmin, J., and Kervarec, N. Modeling [FeFe] Hydrogenase: Synthesis and Protonation of a Diiron Dithiolate Complex Containing a Phosphine-N-Heterocyclic-Carbene Ligand. *Journal of Organometallic Chemistry*, 694(17):2801-2807, 2009. (e) Harb, M. K., Apfel, U. P., Sakamoto, T., El-khateeb, M., and Weigand, W. Diiron Dichalcogenolato (Se and Te) Complexes: Models for the Active Site of [FeFe] Hydrogenase. *European Journal of Inorganic Chemistry*, 2011(7):986-993, 2011.

[2] (a) Adams, M. W. The Structure and Mechanism of Iron-Hydrogenases. *Biochimica et Biophysica Acta (BBA)-Bioenergetics*, 1020(2):115-145, 1990. (b) Garcin, E., Vernede, X., Hatchikian, E. C., Volbeda, A., Frey, M., and Fontecilla-Camps, J. C. The Crystal Structure of a Reduced [NiFeSe] Hydrogenase Provides an Image of the Activated Catalytic Center. *Structure*, 7(5):557-566, 1999. (c) Korbas, M., Vogt, S., Meyer-Klaucke, W., Bill, E., Lyon, E. J., Thauer, R. K., and Shima, S. The Iron-Sulfur Cluster-Free Hydrogenase (Hmd) is a Metalloenzyme with a Novel Iron Binding Motif. *Journal of Biological Chemistry*, 281(41):30804-30813, 2006.

[3] (a) Lubitz, W., Reijerse, E., and Gastel, M. v. [NiFe] and [FeFe] Hydrogenases Studied by Advanced Magnetic Resonance Techniques. *Chemical Reviews*, 107(10):4331-4365, 2007. (b) Fontecilla-Camps, J. C., Volbeda, A., Cavazza, C., and Nicolet, Y. Structure/Function Relationships of [NiFe]-and [FeFe]-Hydrogenases. *Chemical Reviews*, 107(11):4273−4303, 2007. (c) Tard, C. and Pickett, C. J. Structural and Functional Analogues of the Active Sites of the [Fe]-,[NiFe]-, and [FeFe]-Hydrogenases. *Chemical Reviews*, 109(6):2245-2274, 2009. (d) Lubitz, W., Ogata, H., Rüdiger, O., and Reijerse, E. Hydrogenases. *Chemical Reviews*, 114(8):4081-4148,

2014. (e) Simmons, T. R., Berggren, G., Bacchi, M., Fontecave, M., and Artero, V. Mimicking Hydrogenases: From Biomimetics to Artificial Enzymes. *Coordination Chemistry Reviews*, 270-271:127-150, 2014.

[4] Frey, M. Hydrogenases: Hydrogen-Activating Enzymes. *ChemBioChem*, 3(2-3):153-160, 2002.

[5] (a) Peters, J. W., Lanzilotta, W. N., Lemon, B. J., and Seefeldt, L. C. X-ray Crystal Structure of the Fe-Only Hydrogenase (CpI) from Clostridium Pasteurianum to 1.8 Angstrom Resolution. *Science*, 282(5395):1853-1858, 1998. (b) Nicolet, Y., Piras, C., Legrand, P., Hatchikian, C. E., and Fontecilla-Camps, J. C. Desulfovibrio Desulfuricans Iron Hydrogenase: The Structure Shows Unusual Coordination to an Active Site Fe Binuclear Center. *Structure*, 7(1):13-23, 1999.

[6] (a) Schilter, D. and Rauchfuss, T. B. And the Winner is…Azadithiolate: An Amine Proton Relay in the [FeFe] Hydrogenases. *Angewandte Chemie International Edition*, 52(51):13518-13520, 2013. (b) Adamska-Venkatesh, A., Roy, S., Siebel, J. F., Simmons, T. R., Fontecave, M., Artero, V., and Lubitz, W. Spectroscopic Characterization of the Bridging Amine in the Active Site of [FeFe] Hydrogenase Using Isotopologues of the H-Cluster. *Journal of the American Chemical Society*, 137(40):12744-12747, 2015.

[7] (a) Chen, Z., Lemon, B. J., Huang, S., Swartz, D. J., Peters, J. W., and Bagley, K. A. Infrared Studies of the CO-Inhibited Form of the Fe-Only Hydrogenase from Clostridium Pasteurianum I: Examination of Its Light Sensitivity at Cryogenic Temperatures. *Biochemistry*, 41(6):2036-2043, 2002. (b) Roseboom, W., De Lacey, A. L., Fernandez, V. M., Hatchikian, E. C., and Albracht, S. P. The Active Site of the [FeFe]-Hydrogenase from Desulfovibrio Desulfuricans. II. Redox Properties, Light Sensitivity and CO-Ligand Exchange as Observed by Infrared Spectroscopy. *Journal of Biological Inorganic Chemistry*, 11(1):102-118, 2006.

[8] (a) De Lacey, A. L., Fernández, V. M., Rousset, M., and Cammack, R. Activation and Inactivation of Hydrogenase Function and the Catalytic Cycle: Spectroelectrochemical Studies. *Chemical Reviews*, 107(10):4304-4330, 2007. (b) Siegbahn, P. E., Tye, J. W., and Hall, M. B. Computational Studies of [NiFe] and [FeFe] Hydrogenases. *Chemical Reviews*, 107(10):4414-4435, 2007.

[9] (a) Bourrez, M., Steinmetz, R., and Gloaguen, F. Mechanistic Insights into the Catalysis of Electrochemical Proton Reduction by a Diiron Azadithiolate Complex. *Inorganic Chemistry*, 53(19):10667-10673, 2014. (b) Olsen, M. T., Barton, B. E., and Rauchfuss, T. B. Hydrogen Activation by Biomimetic Diiron Dithiolates. *Inorganic Chemistry*, 48(16):7507-7509, 2009. (c) Liu, C., Peck, J. N., Wright, J. A., Pickett, C. J., and Hall, M. B. Density Functional Calculations on Protonation of the [FeFe]-Hydrogenase Model Complex $Fe_2(\mu\text{-pdt})(CO)_4(PMe_3)_2$ and Subsequent Isomerization Pathways. *European Journal of Inorganic Chemistry*, 2011(7):1080-1093, 2011. (d) Camara, J. M. and Rauchfuss, T. B. Combining Acid–Base, Redox and Substrate Binding Functionalities to Give a Complete Model for the [FeFe]-Hydrogenase. *Nature Chemistry*, 4(1):26-30, 2012. (e) Wang, Y. and Ahlquist, M. S. Mechanistic Studies on Proton Transfer in a [FeFe] Hydrogenase Mimic Complex. *Dalton Transactions*, 42(21):7816-7822, 2013. (f) Greco, C. H_2 Binding and Splitting on a New-Generation [FeFe]-Hydrogenase Model Featuring a Redox-Active Decamethylferrocenyl Phosphine Ligand: A Theoretical Investigation. *Inorganic Chemistry*, 52(4):1901-1908, 2013. (g) Bourrez, M., Steinmetz, R., and Gloaguen, F. Mechanistic Insights into the Catalysis of Electrochemical Proton Reduction by a Diiron Azadithiolate Complex. *Inorganic Chemistry*, 53(19):10667-10673, 2014. (h) Wang, W., Rauchfuss, T. B., Zhu, L., and Zampella, G. New Reactions of Terminal Hydrides on a Diiron Dithiolate. *Journal of the American Chemical Society*, 136(15):5773-5782, 2014. (i) Huynh, M. T., Wang, W., Rauchfuss, T. B., and Hammes-Schiffer, S. Computational Investigation of [FeFe]-Hydrogenase Models: Characterization of Singly and Doubly Protonated Intermediates and Mechanistic Insights. *Inorganic Chemistry*, 53(19):10301-10311, 2014.

[10] (a) Munery, S., Capon, J. F., De Gioia, L., Elleouet, C., Greco, C., Pétillon, F. Y., Schollhammer, P., Talarmin, J., and Zampella, G. New Fe^{I}–Fe^{I} Complex Featuring a Rotated Conformation Related to the $[2Fe]_H$ Subsite of [Fe–Fe] Hydrogenase. *Chemistry-A European Journal*, 19(46):15458-15461, 2013. (b) Wang, W., Rauchfuss, T. B., Moore, C. E., Rheingold, A. L., De Gioia, L., and Zampella, G. Crystallographic Characterization of a Fully Rotated, Basic Diiron Dithiolate: Model for the H_{red} State. *Chemistry-A European Journal*, 19(46):15476-15479, 2013. (c) Goy, R., Bertini, L., Elleouet, C., Görls, H., Zampella, G., Talarmin, J., De Gioia, L., Schollhammer, P.,

Apfel, U. P., and Weigand, W. A Sterically Stabilized Fe^{I}–Fe^{I} Semi-Rotated Conformation of [FeFe] Hydrogenase Subsite Model. *Dalton Transactions*, 44(4):1690-1699, 2015.

[11] Zhao, Y. and Truhlar, D. G. The M06 Suite of Density Functionals for Main Group Thermochemistry, Thermochemical Kinetics, Noncovalent Interactions, Excited States, and Transition Elements: Two New Functionals and Systematic Testing of Four M06-Class Functionals and 12 Other Functionals. *Theoretical Chemistry Accounts*, 120(1-3):215-241, 2008.

[12] (a) Weigend, F. Accurate Coulomb-Fitting Basis Sets for H to Rn. *Physical Chemistry Chemical Physics*, 8(9):1057-1065, 2006. (b) Weigend, F.and Ahlrichs, R. Balanced Basis Sets of Split Valence, Triple Zeta Valence and Quadruple Zeta Valence Quality for H to Rn: Design and Assessment of Accuracy. *Physical Chemistry Chemical Physics*, 7(18):3297-3305, 2005.

[13] (a) Tomasi, J., Mennucci, B., and Cammi, R. Quantum Mechanical Continuum Solvation Models. *Chemical Reviews*, 105(8):2999-3094, 2005. (b) Cossi, M., Scalmani, G., Rega, N., and Barone, V. New Developments in the Polarizable Continuum Model for Quantum Mechanical and Classical Calculations on Molecules in Solution. *The Journal of Chemical Physics*, 117(1):43-54, 2002.

[14] (a) Reed, A. E., Curtiss, L. A., and Weinhold, F. Intermolecular Interactions from a Natural Bond Orbital, Donor-Acceptor Viewpoint. *Chemical Reviews*, 88(6):899-926, 1988. (b) Glendening, E. D., Reed, A. E., Carpenter, J. E., and Weinhold, F. NBO Program 3.1, W. T. Madison: 1988.

[15] Frisch, M. J., Trucks, G. W., Schlegel, H. B., Scuseria, G. E., Robb, M. A., Cheeseman, J. R., Montgomery, Jr., J. A., Vreven, T., Kudin, K. N., Burant, J. C., Millam, J. M., Iyengar, S. S., Tomasi, J., Barone, V., Mennucci, B., Cossi, M., Scalmani, G., Rega, N., Petersson, G. A., Nakatsuji, H., Hada, M., Ehara, M., Toyota, K., Fukuda, R., Hasegawa, J., Ishida, M., Nakajima, T., Honda, Y., Kitao, O., Nakai, H., Klene, M., Li, X., Knox, J. E., Hratchian, H. P., Cross, J. B., Bakken, V., Adamo, C., Jaramillo, J., Gomperts, R., Stratmann, R. E., Yazyev, O., Austin, A. J., Cammi, R., Pomelli, C., Ochterski, J. W., Ayala, P. Y., Morokuma, K., Voth, G. A., Salvador, P., Dannenberg, J. J., Zakrzewski, V. G., Dapprich, S., Daniels, A. D., Strain, M. C., Farkas, O., Malick, D.

K., Rabuck, A. D., Raghavachari, K., Foresman, J. B., Ortiz, J. V., Cui, Q., Baboul, A. G., Clifford, S., Cioslowski, J., Stefanov, B. B., Liu, G., Liashenko, A., Piskorz, P., Komaromi, I., Martin, R. L., Fox, D. J., Keith, T., Al-Laham, M. A., Peng, C. Y., Nanayakkara, A., Challacombe, M., Gill, P. M. W., Johnson, B., Chen, W., Wong, M. W., Gonzalez, C., and Pople, J. A. *Gaussian 09*, Revision D.01, Gaussian, Inc., Wallingford CT, 2009.

[16] Neese, F. The ORCA Program System. *Wiley Interdisciplinary Reviews: Computational Molecular Science*, 2(1):73-78, 2012.

[17] (a) Becke, A. D. Density-Functional Thermochemistry. III. The Role of Exact Exchange. *The Journal of Chemical Physics*, 98(7):5648-5652, 1993. (b) Lee, C., Yang, W., and Parr, R. G. Development of the Colle-Salvetti Correlation-Energy Formula into a Functional of the Electron Density. *Physical Review B*, 37(2):785-789, 1988. (c) Vosko, S. H., Wilk, L., and Nusair, M. Accurate Spin-Dependent Electron Liquid Correlation Energies for Local Spin Density Calculations: A Critical Analysis. *Canadian Journal of Physics*, 58(8):1200-1211, 1980.

[18] Schäfer, A., Huber, C., and Ahlrichs, R. Fully Optimized Contracted Gaussian Basis Sets of Triple Zeta Valence Quality for Atoms Li to Kr. *The Journal of Chemical Physics*, 100(8):5829-5835, 1994.

[19] (a) Neese, F. Prediction and Interpretation of the ^{57}Fe Isomer Shift in Mössbauer Spectra by Density Functional Theory. *Inorganica Chimica Acta*, 337:181-192, 2002. (b) Sinnecker, S., Slep, L. D., Bill, E., and Neese, F. Performance of Nonrelativistic and Quasi-Relativistic Hybrid DFT for the Prediction of Electric and Magnetic Hyperfine Parameters in ^{57}Fe Mössbauer Spectra. *Inorganic Chemistry*, 44(7):2245-2254, 2005.

[20] Roemelt, M., Ye, S., and Neese, F. Calibration of Modern Density Functional Theory Methods for the Prediction of ^{57}Fe Mössbauer Isomer Shifts: Meta-GGA and Double-Hybrid Functionals. *Inorganic Chemistry*, 48(3):784-785, 2009.

[21] (a) Becke, A. D. Density-Functional Exchange-Energy Approximation with Correct Asymptotic Behaviour. *Physical Review A*, 38(6):3098-3100, 1988. (b) Perdew, J. P. Density-Functional Approximation for the Correlation Energy of the Inhomogeneous Electron Gas. *Physical Review B*, 33(12):8822, 1986.

[22] Greco, C., Fantucci, P., De Gioia, L., Suarez-Bertoa, R., Bruschi, M., Talarmin, J., and Schollhammer, P. Electrocatalytic Dihydrogen Evolution Mechanism of $[Fe_2(CO)_4(\kappa^2\text{-}Ph_2PCH_2CH_2PPh_2)(\mu\text{-}S(CH_2)_3S)]$ and Related Models of the [FeFe]-Hydrogenases Active Site: a DFT Investigation. *Dalton Transactions*, 39(31):7320-7329, 2010.

[23] Carroll, M. E., Barton, B. E., Rauchfuss, T. B., and Carroll, P. J. Synthetic Models for the Active Site of the [FeFe]-Hydrogenase: Catalytic Proton Reduction and the Structure of the Doubly Protonated Intermediate. *Journal of the American Chemical Society*, 134(45):18843-18852, 2012.

[6.1] List of Publications/Book Chapter:

[1] **Borthakur, B**., Rahman, T., and Phukan, A. K. Tuning the Electronic and Ligand Properties of Remote Carbenes: A Theoretical Study. *The Journal of Organic Chemistry*, 79(22):10801−10810, 2014.

[2] Guha, A. K., **Borthakur, B**., and Phukan, A. K. Spectroscopic Distinction of Different Carbon Bases: An Insight from Theory. *The Journal of Organic Chemistry*, 80(14):7301−7304, 2015.

[3] **Borthakur, B**. and Phukan, A. K. Moving toward Ylide-Stabilized Carbenes. *Chemistry–A European Journal*, 21(32):11603−11609, 2015.

[4] Bharadwaz, P., **Borthakur**, **B**., and Phukan, A. K. Annulated Boron Substituted N-Heterocyclic Carbenes: Theoretical Prediction of Highly Electrophilic Carbenes. *Dalton Transactions*, 44(42):18656–18664, 2015.

[5] **Borthakur**, **B**., Silvi, B., Dewhurst, R. D., and Phukan, A. K. Theoretical Strategies Toward Stabilization of Singlet Remote N-Heterocyclic Carbenes. *Journal of Computational Chemistry*, 37(16):1484–1490, 2016.

[6] **Borthakur**, **B**., Guha, A. K., and Phukan, A. K. Nature of Transannular Interaction in Heavier Group 13 (In, Tl) Atranes: A Theoretical Study. *Polyhedron*, 125:113–121, 2017.

[7] Nutz, M., **Borthakur**, **B**., Dewhurst, R. D., Deißenberger, A., Dellermann, T., Schäfer, M., Krummenacher, I., Phukan, A. K., and Braunschweig, H. Synthesis and Trapping of Iminoboranes by M=B/C=N Bond Metathesis. *Angewandte Chemie International edition*, 56(27):7975–7979, 2017.

[8] Nutz, M., **Borthakur**, **B**., Pranckevicius, C., Dewhurst, R. D., Schäfer, M., Dellermann, T., Glaab, F., Thaler, M., Phukan, A. K., and Braunschweig, H. Release of Isonitrile-and NHC-Stabilized Borylenes from Group VI Terminal Borylene Complexes. *Chemistry–A European Journal*, 24(26):6843-6847, 2018.

[9] **Borthakur**, **B**., Das, S., and Phukan, A. K. Strategies Toward Realization of Unsupported Transition Metal–Boron Donor–Acceptor Complexes: An Insight from Theory. *Chemical Communications*, 54(39):4975-4978, 2018.

[10] **Borthakur**, **B**., Vargas, A., and Phukan, A. K. A Computational Study of Carbene Ligand Stabilization of Biomimetic Models of the Rotated H_{red} State of [FeFe]-Hydrogenase. *European Journal of Inorganic Chemistry*, 2019(17):2295-2303, 2019.

[11] **Borthakur**, **B**. and Phukan, A. K. Can Carbene Decorated [FeFe]-Hydrogenase Model Complexes Catalytically Produce Dihydrogen? An Insight from Theory. *Dalton Transactions*, DOI: 10.1039/C9DT01855G, 2019.

[12] Rohman, S. S., Sarmah, B., **Borthakur, B**., Remya, G. S., Suresh, C. H., and Phukan, A. K. Extending the Library of Boron Bases: A Contribution from Theory. *Organometallics*, Accepted for Publication.

[13] **Borthakur**, **B**. and Phukan, A. K. Structure and Reactivity of Carbones and Ylide Stabilized Carbenes: Contributions from Theory. In Gessner, V. H., Editor, *Modern Ylide Chemistry: Applications in Ligand Design, Organic and Catalytic Transformations*. Volume 177 of *Structure and Bonding*, pages 1-24, 978-3-319-89544-4. Springer International Publishing AG, Cham, Switzerland.

[6.2] List of Conference/Workshop attended:

[1] Attended Regional Training Programme Cum Workshop on ShodhGanga and Anti-Plagiarism Software held at Tezpur University in November, 2014.

[2] Presented poster in the 17th CRSI National Symposium in Chemistry held at CSIR-National Chemical laboratory, Pune in February, 2015.

[3] Participated in the 67th Lindau Nobel Laureate Meeting dedicated to Chemistry held at Lindau, Germany in June, 2017.

[4] Presented poster in the International Conference on Emerging Trends in Chemical Sciences (ETCS) held at Department of Chemistry, Dibrugarh University in February, 2018.

[5] Presented poster in Organix-2018, An International Conference in Chemistry organized by Department of Chemical Sciences, Tezpur University in December, 2018.